HAL
open science

A multi-tone high efficient bandwidth system with an eliminated even-order distortions using double dual-parallel Mach-Zehnder modulator

Taimur Mirza, Shyqyri Haxha, Iyad Dayoub

▶ To cite this version:

HAL Id: hal-03507869

https://hal.science/hal-03507869

Submitted on 19 May 2022

A multi-tone high efficient bandwidth system with an eliminated even-order distortions using double dual-parallel Mach-Zehnder modulator

Taimur N. Mirza [a], Shyqyri Haxha [a,*], Iyad Dayoub [b]

[a] *Department of Electronic Engineering, Royal Holloway University of London, Egham, Surrey TW20 0EX, United Kingdom*
[b] *Iyad Dayoub is with the Institute of Electronic, Microelectronic & Nanotechnology (IEMN CNRS), Université de Valenciennes et du Hainaut-Cambrésis Le Mont-Houy, France*

A B S T R A C T

In this paper, a linearization of dual RF channels over a single carrier wavelength is proposed and experimentally demonstrated. Multiple microwave signals with a multi-octave bandwidth are modulated by a double dual-parallel Mach-Zehnder modulator (D-DPMZM) and recovered by a differential balanced detector (BPD). The theoretical and experimental model illustrates the elimination of second-order harmonic distortions (SHD) and second-order intermodulation (IMD2), and significant suppression of the third-order intermodulation (IMD3) by controlling the phase of the input RF signal and DPMZM. The proposed photonic link configuration illustrates the modulation of two microwave signals on a single optical carrier wavelength, and each RF channel is tested for Two-tone signals to illustrate the linearization of the channelized analog photonic link (CAPL). Firstly, a mathematical model is presented to illustrate the elimination of optical carrier and even-order distortions by using only single-tone in each RF channel. Secondly, the purity of the system is mathematically and experimentally investigated by introducing two-tones in each RF channel. We have analyzed both test cases, with single-tone and with a two-tone test, to help us understand and compare the performance of the system. For test case 1 and test case 2 of our proposed configuration, we have achieved a fundamental signal-to-interference ratio (S/I) of 60 dB and 65 dB with a spurious-free dynamic range (SFDR) of 110 dB.Hz$^{2/3}$ and 116 dB.Hz$^{2/3}$, respectively.

1. Introduction

Analog Photonic links (APLs) deploying external modulators offer great advantages for transmission of microwave signal due to their inherent high bandwidth, high dynamic range, reliability, and immunity to electromagnetic interference (Yao, 2009; Ridgway et al., 2014; Capmany and Novak, 2007; Urick, 2010; Inoue et al., 2016; Paloi et al., 2018). In particular, APLs have great importance in the telecommunication and defense sectors, where they are used for specific applications such as antenna remoting, radar detection, satellite communications, signal generation, and electronic warfare systems. In such APLs, it is essential to channelize the radio frequencies (RF) in order to enable the high-resolution monitoring process (Yao, 2009; Ridgway et al., 2014; Capmany and Novak, 2007; Urick, 2010; Inoue et al., 2016; Paloi et al., 2018). Modulation of multiple RF signals over an optical carrier experience some limitations due to the intermodulation and cross modulation generated by the nonlinearities occurring in optical devices such as

Mach-Zehnder modulator (Xie et al., 2012; Shaqiri and Haxha, 2020). In addition, these nonlinearities also contribute in the generation of multiple distortion products, such as second- and third-order harmonic distortions (SHD and THD), and second- and third-order intermodulation distortions (IMD2 and IMD3). Existence of these nonlinearities have an adverse effect on the spurious-free dynamic range (SFDR). Various techniques have been reported by the scientific community to minimize such distortions; however, these are often sub-octave in nature, which reduces their effectiveness in military and commercial applications (Chen et al., 2013; Wang et al., 2015; Li et al., 2014; Cui et al., 2013a; Li et al., 2013; Jiang et al., 2015).

In the past, most of the research work has reported an improvement of SFDR by suppressing IMD3 and ignoring other distortion products. Though there are various techniques reporting the suppression of IMD2 and IMD3, but these has been unable to demonstrate a simultaneous suppression. Therefore, a main reason of selecting IMD3 has been due to the existence of these frequencies close to the fundamental frequencies,
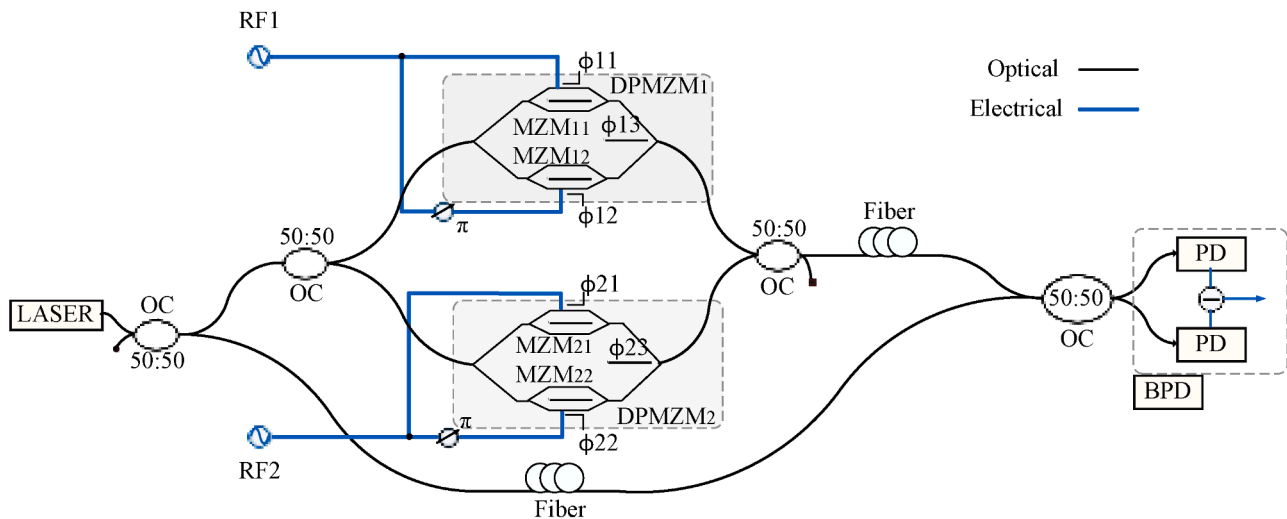
Fig. 1. Schematic diagram of proposed linearization scheme with two input frequencies. OC: Optical Coupler; EDFA: Erbium-doped fiber amplifier; PD: Photodiode; BPD: Balanced Photodetector.

which essentially limits the SFDR and signal bandwidth. A number of modulation techniques have been reported for the system linearization such as using phase modulations (Chen et al., 2013), intensity modulation by using Dual-Electrode MZM (DEMZM) (Wang et al., 2015; Li et al., 2014; Cui et al., 2013a) and Dual-Parallel Mach-Zehnder Modulators (DPMZM) (Li et al., 2013; Jiang et al., 2015; Stewart and Blaylock, Nov 2004; Cui et al., 2013b). In (Chen et al., 2013), an experimental demonstration of linearized APL is reported, which significantly suppresses the IMD3 and IMD2. However, the model does not allow a simultaneous suppression of the IMD3 and IMD2, and it needs to be re-configured for each system optimization. It also requires a further adjustment to its phase modulator and alignment of a polarizer. In (Wang et al., 2015), a two-path structure is demonstrated. The first path modulates the RF signals, and the second path induces a phase shift in the optical carrier. Both paths are combined and then demodulated to achieve a suppression of IMD3. However, it does not present a third-order SFDR, and it only shows a performance of fifth-order SFDR. It is also limited to a precise adjustment in the optical phase between the two paths to achieve the IMD3 cancellation. In (Li et al., 2014), an analog system configuration based on a DEMZM and a balanced photodetector (BPD) is reported. It theoretically demonstrates the elimination of SHD and suppression of the IMD3 by 46 dB. This configuration is complex and difficult to implement in real-life applications. In (Cui et al., 2013a), optical carrier band processing technique is analyzed. It illustrates the suppression of the IMD3 by adjusting the phase of an optical carrier. The reported fundamental to IMD ratio is 64.3 dB, however this scheme is only limited to the sub-octave bandwidth systems. In (Li et al., 2013), Symmetrical Single Sideband (SSB) is realized by using multiple RF phase shifters and Dual-drive MZMs. However, in such systems it is critical to realize the RF phase balance accurately, and any such imbalances would deteriorate the IMD3 cancellation. A similar configuration has also been reported in (Jiang et al., 2015), which eliminates the IMD3 by using multiple RF phase shifter and Dual-drive MZMs. These models do not have the capability of eliminating the second-order distortions, which makes them sub-octave.

To the best of our knowledge, few efforts have been carried out on the multi-octave APL systems as compared to the sub-octave systems. It should also be stated that dual RF channel APL links have not been previously fully explored for performance analysis. We believe that the dual RF channel would have major valuable applications, such as antenna remoting (Stewart and Blaylock, Nov 2004). A multi-octave bandwidth system is presented in (Cui et al., 2013b), however it has not considered the nonlinearities like IMDs. In (Zhu et al., 2016a), a

linearization technique based on a polarization-multiplexing dual-parallel Mach-Zehnder modulator (PM-DPMZM) is reported, which experimentally demonstrates the suppression of the IMD3, IMD2, and SHD. However, its performance is merely dependent on the external bias control and the optical polarization rotator, which is very complicated to control in harsh environmental applications.

In this paper, a linearized method for two RF channels over a single optical wavelength is proposed and investigated theoretically and experimentally. The linearity of the proposed model is investigated by using two-tones in each RF channel, and the suppression of intermodulation distortions are demonstrated. The RF channelization using multiple input signals produces cross modulation and intermodulation distortions (Agarwal et al., 2011; Mendis et al., 1994). However, the proposed models do not contribute to the production of Cross Modulation distortions, which is why it is benchmarked with a single channel modulation system to show a comparison on the linearization of the proposed configuration. In the proposed configuration, the laser beam is split into two equal polarization-maintained paths; the first path includes the modulation link, and the second path consists of a polarization maintained (PM) optical fiber. The modulation link comprises two independent GaAs DPMZMs, and each has a RF phase shifter to cause 180° between two RF inputs of the modulator. Further, the modulated signal with a suppressed carrier is transmitted through the first path, and the optical carrier is traversed through the second path. Both paths are combined by using a 50/50 polarization-maintained coupler and its outputs are connected to a BPD to retrieve the fundamental frequencies of both RF channels. This novel technique, with suppressed optical carrier, proves to be highly efficient as compared to the previously reported linearization techniques, and consequently, a higher suppression of the IMD3 is achieved.

The use of two independent GaAs based DPMZMs as opposed to LiNbO$_3$ offers additional benefits, such as thermal stability and less susceptible to bias drift (Walker et al., 2016; Walker et al., 1989). Moreover, this configuration enables the link for an application of remotely located RF antennas (RF Channels) (Stewart and Blaylock, 2002). For the demonstration purpose, two test cases were employed. First case involves the modulation of single-tone at each channel and the second case includes the modulation of two-tones, which subsequently verifies the linearity of RF channels. For a single-tone analysis of the two RF channels, the experimental demonstration shows an SFDR performance of 116 dB Hz$^{2/3}$ and fundamental signal-to-interference ratio (S/I) of 65 dB. However, for a Two-tone analysis, the SFDR and S/I of 110 dB Hz$^{2/3}$ and 60 dB are achieved, respectively. The purpose of
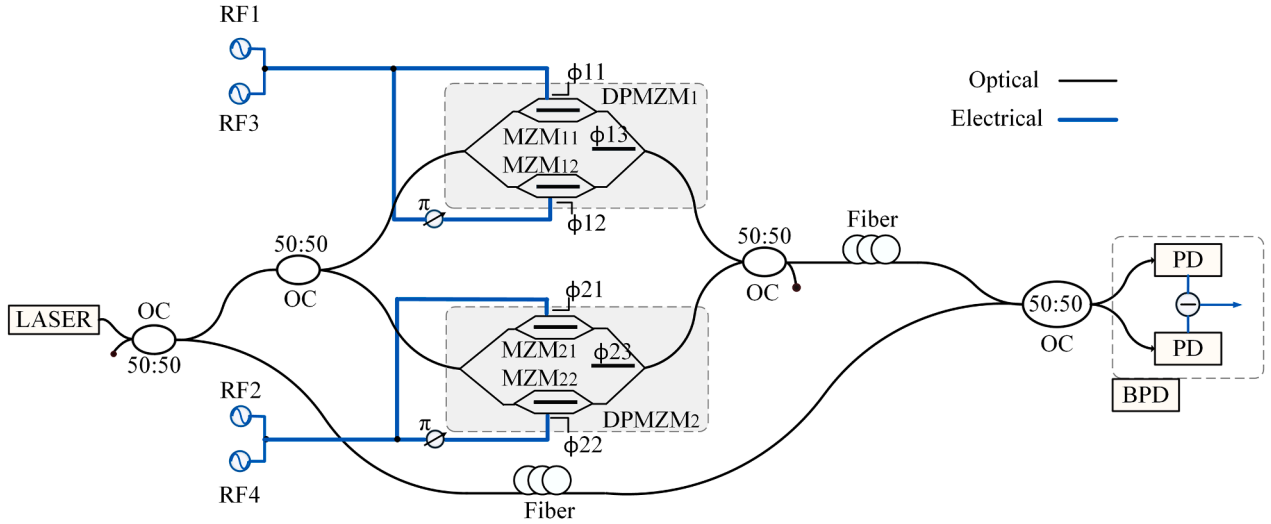
Fig. 2. Schematic diagram of the proposed dual RF channel linearization scheme with four input frequencies.

illustrating these two different case scenarios is to demonstrate the purity of each RF channel in the proposed system.

2. Mathematical model of the proposed system

The schematic diagram of the proposed linearized system with two input tones and four input tones are shown in the Fig. 1 and Fig. 2, respectively. The laser light is injected in a novel monolithic double-dual parallel Mach-Zehnder modulator (D-DPMZM), which is denoted by E_c with its angular frequency of ω_c.

2.1. Suppression of an optical carrier

In this section, a mathematical model of a proposed system is developed, where the optical carrier and even-order harmonics are theoretically eliminated. Initially, a single-tone signal is used in each RF channel to demonstrate the optical carrier suppression, as it is shown in Fig. 1. The D-DPMZM deployed which consists of two dual-parallel MZMs (DPMZM) where each DPMZM is comprised of two sub-MZMs. Both incoming signals; RF1 in channel-1 and RF2 in channel-2 are used as input RF signals in DPMZM1 and DPMZM2, respectively. RF1 and RF2 are mathematically denoted as ω1 and ω2, respectively.

The input RF signal to the upper and lower sub-MZMs of DPMZM$_i$ (i = 1, 2) has a phase difference of 180°, which is achieved by using an RF Phase Shifter. Each MZM$_{ij}$ (i = 1, 2, j = 1, 2, 3) of DPMZM$_i$ (i = 1, 2) are bias controlled to set the operating point at NULL. It is well known that biasing the modulator electrodes to NULL operating point leads to the suppression of optical carrier and even order harmonics. In our proposed model, the purpose of RF phase shifters is to avoid the destructive interference of fundamental sidebands when DPMZM$_i$ (i = 1, 2) is biased to Null operating point. The transfer function of DPMZM$_i$ (i = 1, 2) can be expressed as (Mirza et al., 2021):

$$E_{DPMZM_i}(t) = E_c e^{j\omega_c t}\left[cos\left(\frac{\phi_{i1}(t)}{2}\right) + e^{j\phi_{i3}}cos\left(\frac{\phi_{i2}(t)}{2}\right)\right] \qquad (1)$$

To further simplify (1), a phase difference between the two arms of each MZM$_{ij}$ is$\varnothing_{ij} = \pi V_{biasij}/V_{\pi i}$, which is controlled by the DC bias voltageV_{biasij} and the half-wave voltage$V_{\pi i}$. Each MZM$_{ij}$ is modulated by an RF signalω_{mi}. The phase difference caused by a modulation voltage on MZM$_{i1}$ of ith-DPMZM is$\varnothing_{m_i}(t) = \pi V_i cos(\omega_{m_i})/V_{\pi i}$, and the phase difference on MZM$_{i2}$ with an additional RF phase shift of 180° is$\varnothing'_{m_i}(t) = m_i cos(\omega_{m_i}t + \pi)$, where$m_i = \pi V_i/V_{\pi i}$, consequently, the total phase change of MZM$_{i1}$ can be expressed as;

$$\phi_{i1}(t) = \phi_{m_i}(t) + \phi_{i1} \qquad (2)$$

Likewise, the phase change of MZM$_{i2}$ is shown as;

$$\phi_{i2}(t) = \phi'_{m_i}(t) + \phi_{i2} \qquad (3)$$

Eq. (1) can be further expanded by substituting (2) and (3). It is simplified by applying a Jacobi-Anger Expansion, where high-order Bessel functions are analyzed as below;

$$E_{DPMZM_i}(t) = E_c\left[\begin{array}{c}-2J_1 m_1 cos(\omega_c t)cos(\omega_{m_i}t) \\ +2J_3 m_2 cos(\omega_c t)cos(3\omega_{m_i}t)\end{array}\right] \qquad (4)$$

Where J_1 and J_3 are the first-order and third-order Bessel functions. The resultant electric field of the modulator shows that an optical carrier and even-order harmonics are eliminated, as follows;

$$E_{DPMZM_i}(t) = E_c\left[\begin{array}{c}-J_1 m_1\{cos(\omega_c t + \omega_{m_i}t) + cos(\omega_c t - \omega_{m_i}t)\} \\ +J_3 m_2\{cos(\omega_c t + 3\omega_{m_i}t) + cos(\omega_c t - 3\omega_{m_i}t)\}\end{array}\right] \qquad (5)$$

2.2. Second-order and third-order intermodulation suppression

A further investigation is carried out by introducing two-tone frequencies at each RF channel in the first model (shown in Fig. 1). which is a combination of two RF signals at each input of the DPMZM$_i$, as it is shown in Fig. 2. The DC bias conditions are kept the same as the first model.

At each RF channel, two-tone frequencies are equally spaced from each other with a band of 10 MHz. Like the first model, as in (2) and (3), the two-tones are modulated in each sub-MZM, and the phase difference caused by the modulating voltage is expressed as;

$$\left.\begin{array}{r}\phi_{m1}(t) = m_{11}cos(\omega_{m11}t) + m_{12}cos(\omega_{m12}t) \\ \phi'_{m1}(t) = m_{11}cos(\omega_{m11}t + \pi) + m_{12}cos(\omega_{m12}t + \pi) \\ \phi_{m2}(t) = m_{21}cos(\omega_{m21}t) + m_{22}cos(\omega_{m22}t) \\ \phi'_{m2}(t) = m_{21}cos(\omega_{m21}t + \pi) + m_{22}cos(\omega_{m22}t + \pi)\end{array}\right\} \qquad (6)$$

Where,$\varnothing_{m1}(t)$ and $\varnothing'_{m1}(t)$ are the phase changes occurred due to the RF modulation voltages at the sub-MZMs of DPMZM$_1$ for RF$_1$ and RF$_3$, and similarly, $\varnothing_{m2}(t)$ and $\varnothing'_{m2}(t)$ are the phase change at each sub-MZM of DPMZM$_2$ for RF$_2$ and RF$_4$, respectively. By using (6), this phase information can be substituted into (1) in order to obtain the transfer function of the D-DPMZM with four input frequencies. Hence, the electric field of DPMZM$_1$ and DPMZM$_2$ is expressed in (7) and (8).
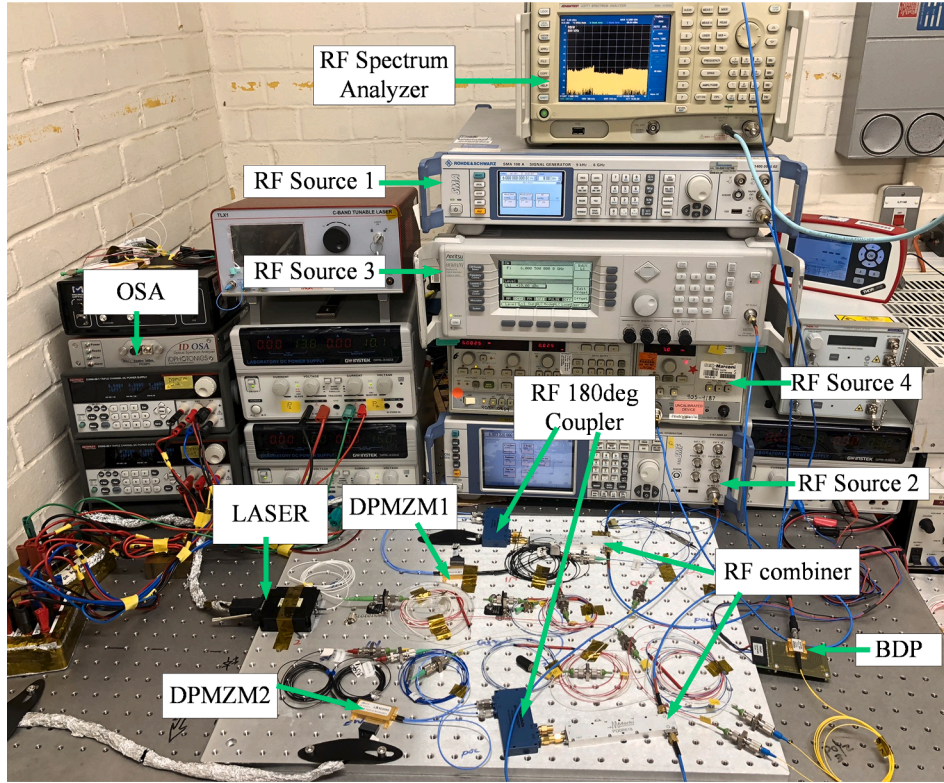
Fig. 3. Experimental setup of the proposed scheme in our microwave photonics lab.

$$E_{DPMZM1}(t) = E_c e^{j\omega_c t} \left[\begin{array}{c} cos\left(\dfrac{[m_{11}cos(\omega_{m11}t) + m_{12}cos(\omega_{m12}t)] + \phi_{11}}{2} \right) + \\ e^{j\phi_{i3}} cos\left(\dfrac{[-m_{11}cos(\omega_{m11}t) - m_{12}cos(\omega_{m12}t)] + \phi_{12}}{2} \right) \end{array} \right]$$

(7)

$$E_{DPMZM2}(t) = E_c e^{j\omega_c t} \left[\begin{array}{c} cos\left(\dfrac{[m_{21}cos(\omega_{m21}t) + m_{22}cos(\omega_{m22}t)] + \phi_{21}}{2} \right) + \\ e^{j\phi_{i3}} cos\left(\dfrac{[-m_{21}cos(\omega_{m21}t) - m_{22}cos(\omega_{m22}t)] + \phi_{22}}{2} \right) \end{array} \right]$$

(8)

The electric field of DPMZM$_1$ and DPMZM$_2$ can be combined to achieve a resultant D-DPMZM electric field, which is expressed as;

$$E_{D-DPMZM}(t) = E_{DPMZM1}(t) + E_{DPMZM2}(t).$$

(9)

Equation (9) can be further expanded by using (7) and (8), hence;

$$E_{D-DPMZM}(t) = E_c e^{j\omega_c t} \left[\begin{array}{c} \left\{ \begin{array}{c} cos\left(\dfrac{\phi_{m1}(t) + \pi}{2} \right) \\ + e^{j\phi_{13}} cos\left(\dfrac{\phi'_{m1}(t) + \pi}{2} \right) \end{array} \right\} \\ + \left\{ \begin{array}{c} cos\left(\dfrac{\phi_{m2}(t) + \pi}{2} \right) \\ + e^{j\phi_{23}} cos\left(\dfrac{\phi'_{m2}(t) + \pi}{2} \right) \end{array} \right\} \end{array} \right]$$

(10)

Bias conditions for all the sub-MZMs are kept the same at a NULL operating point. Since the carrier is suppressed, a coherent receiver is needed to recover the signal in the RF domain (Zhu et al., 2009). An optical carrier is combined with the reference signal by using a directional coupler. The two output fields of the optical coupler are given in

the (11), which is then detected at the BPD (Qin and Jiang, 2015).

$$\begin{bmatrix} E_1(t) \\ E_2(t) \end{bmatrix} = \frac{1}{\sqrt{2}} \begin{bmatrix} E_{D-DPMZM}(t) + jE_L(t) \\ E_L(t) + jE_{D-DPMZM}(t) \end{bmatrix}$$

(11)

The photocurrent $I_{BPD}(t)$ of the BPD can be determined by substituting output fields of the coupler into the following equation:

$$I_{BPD}(t) = \Re \left[E_1(t).E_1^*(t) - E_2(t).E_2^*(t) \right]$$

(12)

Where, $\Re$ is the responsivity of the photodetector, and $E_1(t)$ and $E_2(t)$ are the optical fields of the optical coupler. By using (10) and (11), and setting $\varnothing_{ij} = \pi$, (12) can be rewritten as follows;

$$I_{BPD}(t) = 4\Re E_C E_L \left\{ \begin{array}{c} -2sin\left(\dfrac{\phi_{m1}(t)}{2} \right) \\ -2sin\left(\dfrac{\phi_{m2}(t)}{2} \right) \end{array} \right\} cos((\omega_C - \omega_L)t)$$

(13)

It is known that the Optical carrier angular frequency ω_C and local oscillator angular frequency ω_L are the same. Also, by substituting $\varnothing_{m1}(t)$ and $\varnothing_{m2}(t)$ into (13), hence;

$$I_{BPD}(t) = 4\Re E_C E_L \left\{ \begin{array}{c} -sin\left(\dfrac{m_{11}cos(\omega_{m11}t) + m_{12}cos(\omega_{m12}t)}{2} \right) \\ -sin\left(\dfrac{m_{21}cos(\omega_{m21}t) + m_{22}cos(\omega_{m22}t)}{2} \right) \end{array} \right\}$$

(14)

By applying the Jacobi-Anger Expansion in (14), the high order Bessel functions can be explored to understand the beating of different frequency components, which can be expressed as;

$$I_{BPD}(t) = -4\Re E_C E_L \left\{ \begin{array}{l} \sum_{k,l=-\infty}^{\infty} J_{k,l}\left(\frac{m_{11}}{2}\right)\left(\frac{m_{12}}{2}\right)\left(\frac{m_{21}}{2}\right)\left(\frac{m_{22}}{2}\right) \\ \\ \times \left[\begin{array}{l} sin\left(\begin{array}{l} k\omega_{m11} + l\omega_{m12} \\ \\ +(k+l)\left(\frac{\pi}{2}\right) \end{array} \right) \\ \\ +sin\left(\begin{array}{l} k\omega_{m21} + l\omega_{m22} \\ \\ +(k+l)\left(\frac{\pi}{2}\right) \end{array} \right) \end{array} \right] \end{array} \right\} \quad (15)$$

By expanding (15), the second order intermodulation distortions and second order harmonics can be removed. However, in order to satisfy this condition, the variable "k" is not equal to "l" ($k \neq l$). The Jth order Bessel Function can be expanded up to Fourth order as anything above can be neglected or filtered out by the system Bandwidth., hence;

$$I_{BPD}(t) = -4\Re E_C E_L$$

$$\times \left[\begin{array}{l} J_{0,1}\left(\frac{m_{12}}{2}\right)\left(\frac{m_{22}}{2}\right)(cos(\omega_{m12}t) + cos(\omega_{m22}t)) \\ \\ +J_{1,0}\left(\frac{m_{11}}{2}\right)\left(\frac{m_{21}}{2}\right)(cos(\omega_{m11}t) + cos(\omega_{m21}t)) \\ \\ +J_{1,2}\left(\frac{m_{11}}{2}\right)\left(\frac{m_{12}}{2}\right)\left(\frac{m_{21}}{2}\right)\left(\frac{m_{22}}{2}\right)\left(\begin{array}{l} cos(\omega_{m11} + 2\omega_{m12})t \\ +cos(\omega_{m21} + 2\omega_{m22})t \end{array} \right) \\ \\ +J_{2,1}\left(\frac{m_{11}}{2}\right)\left(\frac{m_{12}}{2}\right)\left(\frac{m_{21}}{2}\right)\left(\frac{m_{22}}{2}\right)\left(\begin{array}{l} cos(2\omega_{m11} + \omega_{m12})t \\ +cos(2\omega_{m21} + \omega_{m22})t \end{array} \right) \\ \\ +J_{-1,2}\left(\frac{m_{11}}{2}\right)\left(\frac{m_{12}}{2}\right)\left(\frac{m_{21}}{2}\right)\left(\frac{m_{22}}{2}\right)\left(\begin{array}{l} cos(2\omega_{m12} - \omega_{m11})t \\ +cos(2\omega_{m22} - \omega_{m21})t \end{array} \right) \\ \\ +J_{2,-1}\left(\frac{m_{11}}{2}\right)\left(\frac{m_{12}}{2}\right)\left(\frac{m_{21}}{2}\right)\left(\frac{m_{22}}{2}\right)\left(\begin{array}{l} cos(2\omega_{m11} - \omega_{m12})t \\ +cos(2\omega_{m21} - \omega_{m22})t \end{array} \right) \end{array} \right]$$

$$(16)$$

From (16), it can be clearly observed that IMD2 and SHD are eliminated. The proposed design perseveres a high dynamic range by keeping IMD3s low, even when a modulator is driven at high RF power. $J_{0,1}$ and $J_{1,0}$ represent the first-order Bessel function, and can be seen in (16) as fundamental RF signals. $J_{1,2}$ and $J_{2,1}$ represent the intermodulation signals produced due to interference between the first-order signals and the second-order signals, which is known as the third-order Intermodulation distortions.

3. Experimental results and discussions

The proposed APL system configuration is developed and implemented experimentally in our microwave photonics and sensors (MPS) lab, inducing its real-life performance demonstration. The experimental setup is illustrated in Fig. 3. It should be stated that all-optical equipment used in the experiment have polarization maintained fiber (PMF) pigtails. The purpose of employing PMFs in the system is to void any disturbance in the state-of-polarization throughout an optical link. A distributed feedback (DFB) laser (Gooch & Housego, EM650-193400-100-PM900-FCA-NA) operating at wavelength of 1550 nm with a maximum optical power of 20dBm, and relative intensity noise (RIN) of −155dBm/Hz, is used as an optical source. The beam is split by a 50/50 polarization-maintained optical coupler (Thorlabs, PN1550R5A2), and then the first half is transmitted through a modulation link, and the other half traversed through a PMF. The modulation link is composed of two independent GaAs DPMZMs (Axenic, aXSD2050), which have a half-wave voltage of 4 V and a bandwidth of 50 GHz. The RF ports in each DPMZM are connected to a 180° hybrid coupler (RF Lambda, RFHB02G18GPI), which induces a phase difference of 180° between the two RF inputs. The input RF signals; RF1 = 6.0005 GHz, RF2 = 6.00328
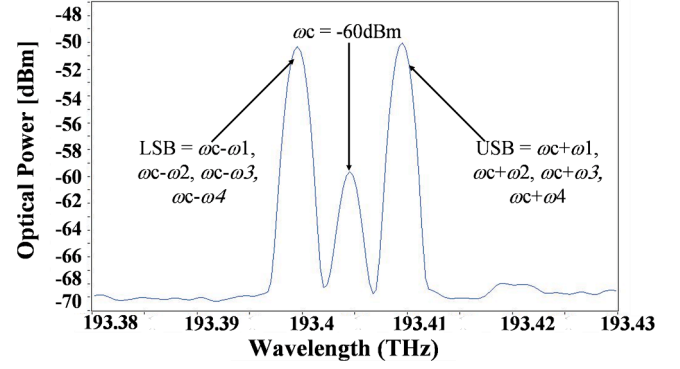

Fig. 4. Measured optical spectrum of a combined optical field from two DPMZMs.

GHz, RF3 = 6 GHz, RF4 = 6.00278 GHz, are generated from the RF signal generators (R&S, SMA100A; R&S, SMF100A; Anritsu, 68369A/NV; Hewlett Packard, 8350B) at an amplitude of 6dBm. It should be stated that the input RF signals are combined by using two power dividers (Marki Microwave, PD-0R618). Both optical paths are joined at 50/50 optical coupler, and each output link of the coupler is connected at the input link of the BPD (Finisar, BPDV2120R-VM-FP). The responsivity level of the BPD is defined as 0.6A/W and 0.63A/W. The BPD is configured to form a differential function by applying an oppositely charged bias on each diode. The length of both optical paths is kept the same, and a slight adjustment is made by using an optical delay line (Oz Optics, ODL-700-11-1550-9/125-S-60-3A3A-1-1), which can induce a delay of up to 18 ps. It should be stated that the intrinsic property of the BPD also helps in reducing the amplified spontaneous emission (ASE) and RIN from the laser (Zhu et al., 2009; Middleton and DeSalvo, 2009).

In a proposed architecture, balanced detection is primarily used to cancel out the SHD and IMD2. Due to the suppression of the optical carrier at the modulator, only sidebands are transmitted through the optical fiber, which requires the BPD to retrieve the transmitted signal. The phase information is not available at the direct detection, whereas balanced detection provides phase and amplitude information of the transmitted signal. As we know, the increase in laser power increases the RIN, which results in the degradation of the signal-to-noise ratio (SNR). However, this degradation of the SNR can be avoided by using the coherent BPD. The benefits of the BPD over a single direct photodetector makes it suitable for the proposed schematics (Kim et al., 2009). The electrical output of the BPD is analyzed by the electrical spectrum analyzer ESA (Advantest, U3771).

Both independent GaAs DPMZMs are bias controlled to achieve maximum suppression of optical carrier, as it is shown in Fig. 4. The suppression is analyzed by using an optical spectrum analyzer (OSA), and the modulator's Null operating position was adjusted by gradually varying the DC voltage. However, the manual handling of DC voltages can be replaced by automated bias controllers (ABC) in future work. In Fig. 4, a suppressed carrier double sideband spectrum is illustrated, which is observed at the output of a coupler that joins the output fields of both DPMZMs. Experimentally, complete elimination of the optical carrier is not possible due to the intrinsic imbalance properties of the modulator. A suppressed carrier double sideband is then transmitted through an optical patch cable and then combined with a pilot optical carrier, which has traversed through an independent polarization-maintained optical fiber. In Fig. 4, upper sideband (USB) and lower sideband (LSB) represent the fundamental input frequencies (RF1 = 6.0005 GHz, RF2 = 6.00328 GHz, RF3 = 6 GHz, RF4 = 6.00278 GHz) of dual RF channel with respect to a central optical carrier frequency of 193.404THz (1550.084 nm).

The combination of two optical paths is then fed to each input of BPD, which is then converted to an electrical signal. We have also analyzed the electrical output signal with the help of a VPI simulation
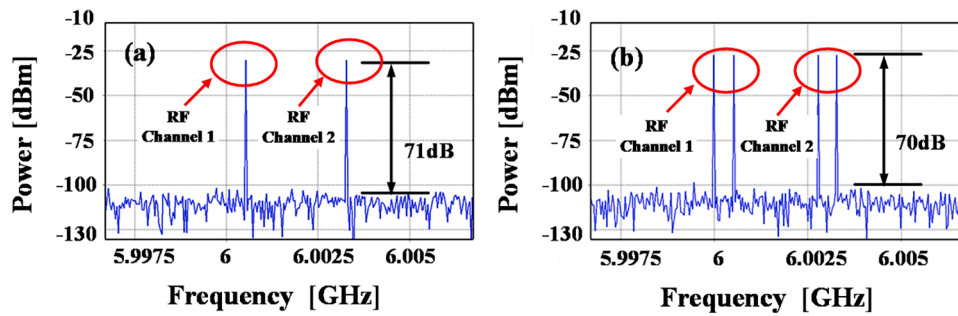
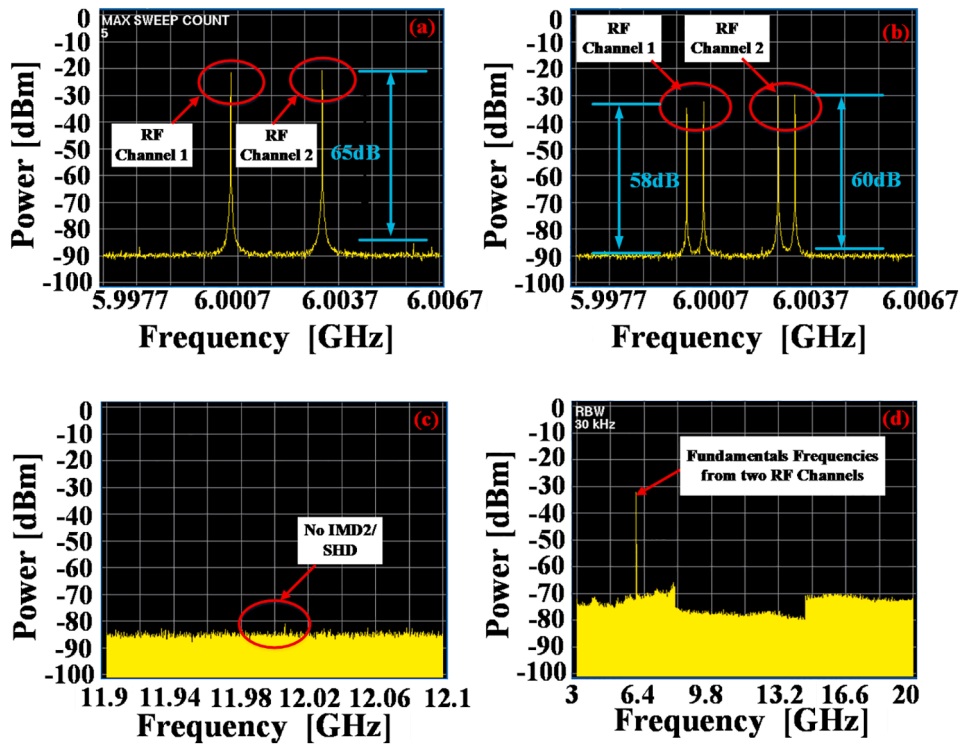**Fig 5.** Simulated Electrical spectrum (a) Single-tone Dual RF channel (b) Two-tone Dual RF channel.

Fig 6. Measured Electrical Spectrum, (a) Single-tone dual RF channel (b) Two-tone dual RF channel (c) Second-order distortions for two-tone test (d) Wide spectrum for a two-tone dual RF channel.

model, and then it was compared with the results achieved from an experiment. In Fig. 5(a), the fundamental single-tone signals of RF channel-1 and RF channel-2 are shown at a frequency of 6.0005 GHz and 6.00328 GHz. The IMD3 produced due to interference between the channels is below the noise floor when the modulation index is kept 0.28. Hence, the signal to interference (S/I) ratio of 71 dB was observed. In Fig. 5(b), fundamental two-tone signals are modulated in each channel and transmitted through an APL. It is noticed that the S/I of 70 dB can be achieved at a modulation index of 0.22. The two-tone signals used in RF channel-1 are 6 GHz and 6.0005 GHz, whereas, in RF channel-2, 6.00328 GHz and 6.00278 GHz are used.

Likewise, the electrical signals received at the BPD are analyzed by an ESA, which itself has some restrictions such as the limited noise power density. However, the results are shown in Fig. 6 has a smaller S/I as compared to the simulated results. It can be clearly illustrated that the performance is mainly limited by the noise floor in the experimental results. Fig. 6(a) shows a single-tone spectrum of dual RF channel, and the measured S/I is 65 dB. IMD3 produced, in this case, are at 5.99772 GHz, and 6.00606 GHz, which has an amplitude of around −85dBm. The fundamental single-tones have a peak power of around −20dBm. It is to
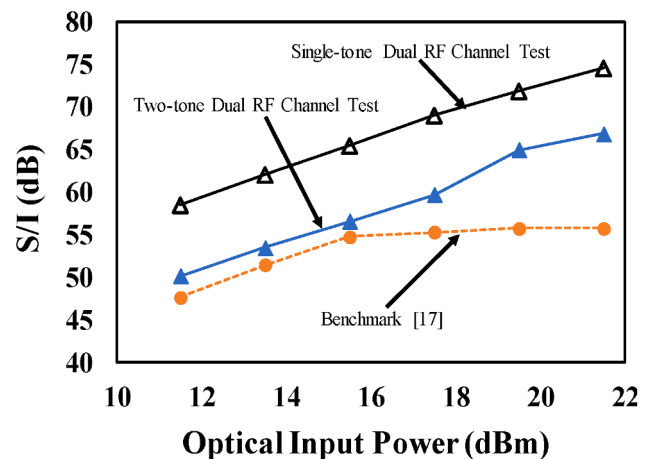

Fig. 7. Performance analysis of a proposed model and the benchmark model, as a reference of Optical input power.
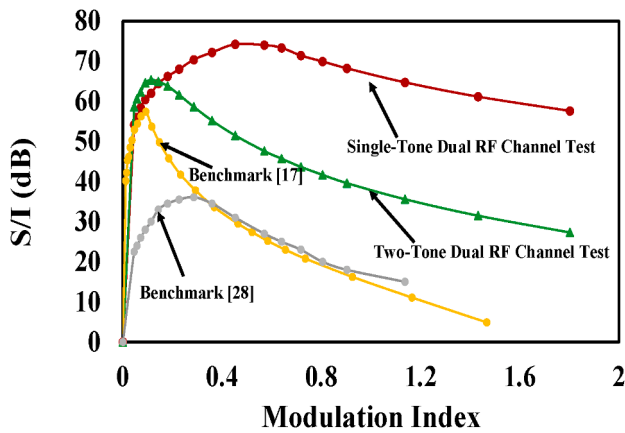
Fig 8. Signal to Interference ratio as a function of Modulation index.

be noted that the input RF power is kept at 6dBm for all tones, which gives a link gain of around −26 dB. Fig. 6(b) shows a two-tone spectrum of dual RF channel with a measured S/I of 60 dB. In this case, RF channel-1 demonstrates a link gain of around −38 dB, whereas RF channel-2 shows a link gain of −36 dB. The two-tone test is further explored in Fig. 6(c) for IMD2 and SHD, which do not appear above the noise floor. To observe the distortions, a wideband spectrum is shown in Fig. 6(d), which depicts the fundamental frequencies and suppressed intermodulation distortions. Different levels of noise floor are due to the internal band filter of the ESA.

After the demodulation process of the transmitted signal, the S/I is plotted with reference to optical input power from the laser and compared with the benchmarked results, as shown in Fig. 7. It should be noted that the benchmark method reported in (Zhu et al., 2016a) has limited S/I due to the existence of high IMD3, whereas the proposed method is much robust and has a potential to achieve S/I of up to ∼75 dB

considering the power limitation posed by the optical devices. However, the S/I for benchmarked PM-DPMZM method reported in (Zhu et al., 2016a) is nearly constant at 15.5dBm. This illustration provides a foreseen optimized performance of the proposed link when the optical source power is increased. The components used in the existing infrastructure of APL are power limited, and high optical power would either deteriorate the performance or damage the component. Therefore, by overcoming the power limitation, the performance of APL can be further improved.

A linear modulation range of the proposed model is investigated by observing the modulation index. At a small modulation index, the system generally has a higher signal-to-interference ratio, and by plotting the data, the linear region of a modulator can be observed. In our proposed model, the modulation index is optimized to achieve a maximum dynamic range. For a single-tone test, the S/I is maximum at a modulation index of 0.57. However, for the Two-Tone linearization test, the S/I of ∼65 dB is achievable at a modulation index of 0.14 (as shown in Fig. 8). Both cases are benchmarked with the previously reported single channel two-tone APL (Zhu et al., 2016a) and the optical carrier suppression with carrier (OCS + C) based APL link (Zhu et al., 2016). Similar symmetry is observed across all cases, as the performance of the model deteriorates at a high modulation index, which means the modulator is being overdriven. Benchmark model shows S/I of 36.2 dB at a modulation index of 0.26, whereas the proposed method can achieve a S/I of upto 70 dB at a modulation index of 0.28.

The SFDR performance of the proposed scheme, based on the linearization tests for the Dual RF channel, is illustrated in Fig. 9. The output RF power of fundamental frequencies and IMD3 as a function of the input RF power is plotted for both Single-tone and two-tone tests. The noise floor based on the laser RIN, photocurrent shot-noise and thermal noise is set to −160dBm/Hz, considering the thermal noise of 3.163e-10A/$\sqrt{Hz}$ at the detector (Mirza et al., 2021). However, the measured noise floor from the ESA is −140dBm/Hz, which is restricted by ESA specifications. In the SFDR measurements, the calculated noise floor of
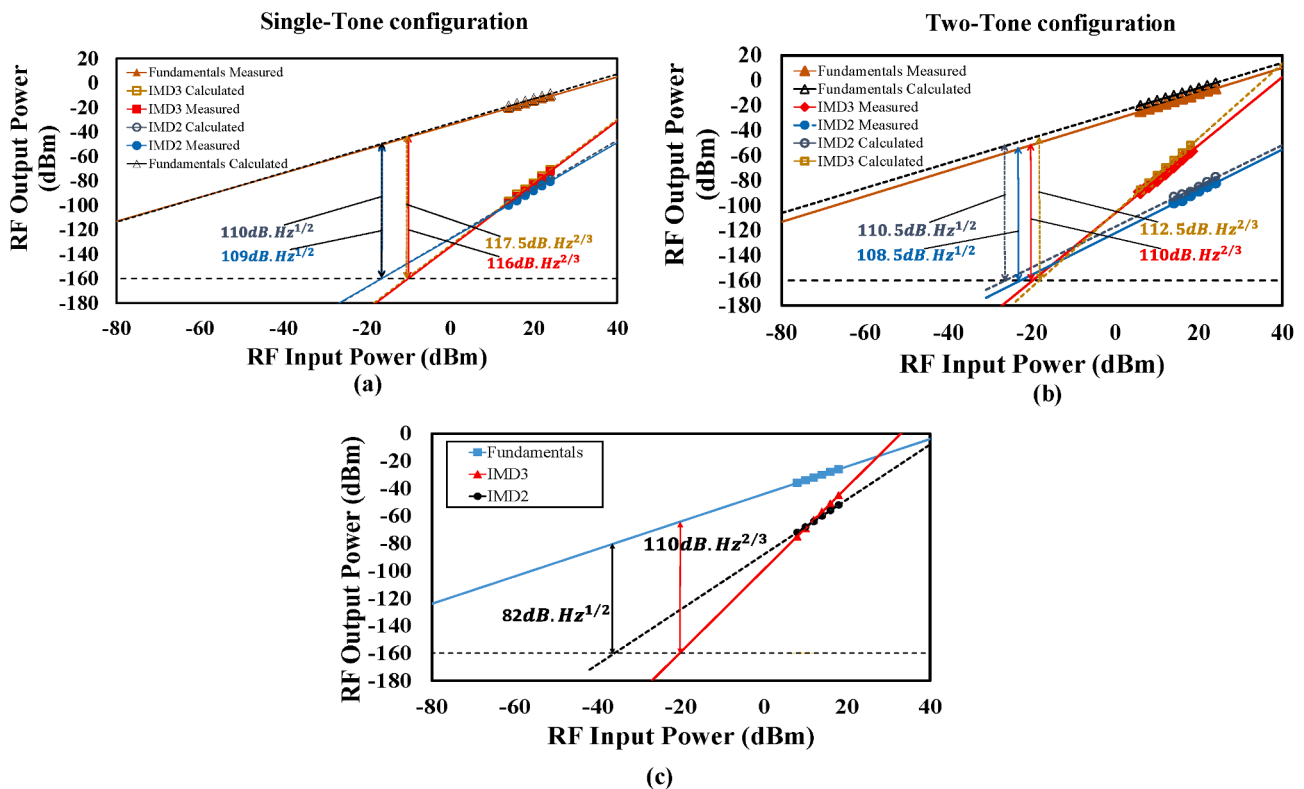

Fig 9. SFDR performance of (a) a proposed D-DPMZM scheme for the linearization of Single-Tone and (b) Two-Tone Dual RF channel, and (c) PM-DPMZM based single RF channel scheme (Zhu et al., 2016a).

−160dBm/Hz is used. All the fundamental frequencies and their IMD3s have an equal output power as the input RF powers for each tone is kept similar, which is then varied to calculate the performance of SFDR. As can be seen from our proposed Single-tone linearization test, we have achieved an SFDR of 116 dB Hz$^{2/3}$, and it is of 110 dB Hz$^{2/3}$ for the two-tone linearization test of a dual RF channel, which is 6 dB higher than the PM-DPMZM based system (Zhu et al., 2016a). Although, the system used in (Zhu et al., 2016a) is a single channel, the performance of our proposed dual channel system is much better. Fig. 9(a) shows the measured and calculated SFDR performance of the proposed model with a Single-tone input signal at each RF channel. The measured SFDR2 and SFDR3 for a single-tone test are 1 dB and 1.5 dB lower than the calculated values, respectively. This demonstrates that single-tone in two RF channels behave linearly. Whereas, for our two-tone test, the calculated SFDR2 and SFDR3 are 2 dB and 2.5 dB higher than the measured experimental values, respectively as it is shown in Fig. 9(b). It is to be noted that in both cases, the SFDR2 is comparatively high, which illustrates that IMD2s have been highly suppressed. Fig. 9(c) shows the SFDR2 and SFDR3 performance of a single channel PM-DPMZM based system is 82 dB Hz$^{1/2}$ and 110 dB Hz$^{2/3}$, respectively.

The proposed linearized scheme realizes a highly efficient multi-tone dual-channel system. However, biasing the multiple modulators to a desired operating point can be a bit tricky, which can be omitted by using automated bias controllers (ABC) in a real experiment. The performance can be further improved by using amplified spontaneous emission (ASE) filters to reduce the noise level after the amplification of an optical signal.

4. Conclusion

A highly linearized APL with two RF channels, based on a D-DPMZM, has been developed and demonstrated. The proposed APL configuration has been validated for two test performance scenarios, where initially only single RF tone was modulated in each channel, known as single-tone test. In the second test scenario, two-tones were modulated in each channel, which is known as two-tone test. The proposed architecture was mathematically validated and then it was developed in a VPI simulation software. The model has been experimentally demonstrated, and it was proved that by suppressing the optical carrier at modulation stage, the linearization of APL can be highly improved. It was discovered that the main performance contributing factors in the proposed APL are; RF phase difference of 180 deg between two sub-MZMs of each DPMZM, adjusting the MZM imbalance, nulling the optical carrier by appropriately biasing the modulators, and input power to the BPD. The proposed double dual-parallel MZM can be realized for a multi-tone dual RF channels and a multi-octave bandwidth system over a single optical wavelength. The performance of two Channels is tested by using single-tone and two-tone tests, which has exhibited an SFDR3 of 116 dB Hz$^{2/3}$, SFDR2 of 109 dB Hz$^{1/2}$, and S/I of up to 65 dB for a single-tone test. The SFDR3, SFDR2, and S/I of 110 dB Hz$^{2/3}$, 108.5 dB Hz$^{1/2}$, and 60 dB, are measured for two-tone test, respectively. The proposed APL configuration have great impact on RF signal channelization, and it would also have significant potential on transmitting more than four-tones, which can be pursued for future work.

Declaration of Competing Interest

The authors declare that they have no known competing financial interests or personal relationships that could have appeared to influence the work reported in this paper.

Acknowledgment

References

Yao, J., 2009. Microwave Photonics. Journal of Lightwave Technology 27 (3), 314–335.

Ridgway, R.W., Dohrman, C.L., Conway, J.A., 2014. Microwave Photonics Programs at DARPA. Journal of Lightwave Technology 32 (20), 3428–3439.

Capmany, J., Novak, D., 2007. Microwave photonics combines two worlds. Nat. Photonics 1 (6), 319–330.

V. J. Urick, "Long-haul analog links tutorial," *Optical Fiber Communication (OFC), collocated National Fiber Optic Engineers Conference, 2010 Conference on (OFC/NFOEC)*, San Diego, CA, pp. 1-39, 2010.

Inoue, D., Hiratani, T., Fukuda, K., Tomiyasu, T., Amemiya, T., Nishiyama, N., Arai, S., 2016. Low-bias current 10 Gbit/s direct modulation of GaInAsP/InP membrane DFB laser on silicon. Opt. Express 24 (16), 18571–18579.

Paloi, F., Haxha, S., Mirza, T.N., Alom, M.S., 2018. Microwave Photonic Downconversion With Improved Conversion Efficiency and SFDR. IEEE Access 6, 8089–8097.

X. Xie, Y. Dai, Y. Ji, K. Xu, Y.Li, J. Wu and J. Lin, "Broadband Photonic Radio-Frequency Channelization Based on a 39-GHz Optical Frequency Comb," in *IEEE Photonics Technology Letters*, vol. 24, no. 8, pp. 661-663, April15, 2012.

Shaqiri, S., Haxha, S., 2020. Linearization and Down-Conversion of Microwave Photonics Signal based on Dual-drive Dual-parallel Mach-Zehnder Modulator with Eliminated 3rd Intermodulation and 2nd Distortions. Optik 204 (164103), Feb.

Chen, Z., Yan, L., Pan, W., Luo, B., Zou, X., Guo, Y., Jiang, H., Zhou, T., 2013. SFDR enhancement in analog photonic links by simultaneous compensation for dispersion and nonlinearity. Opt. Express 21 (18), 20999–21009.

Wang, S., Gao, Y., Wen, A., Liu, L., 2015. A microwave photonic link with high spurious-free dynamic range based on a parallel structure. Optoelectron. Lett. 11 (2), 137–140.

Li, Xuan, Zhu, Zihang, Zhao, Shanghong, Li, Yongjun, Han, Lei, Zhao, Jing, 2014. An intensity modulation and coherent balanced detection intersatellite microwave photonic link using polarization direction control. Optics & Laser Technology 56, 362–366.

Cui, Y., Dai, Y., Yin, F., Dai, J., Xu, K., Li, J., Lin, J., 2013a. Intermodulation distortion suppression for intensity-modulated analog fiber-optic link incorporating optical carrier band processing. Opt. Express 21 (20), 23433–23440.

Li, J., Zhang, Y., Yu, S., Jiang, T., Xie, Q., Gu, W., 2013. Third-order intermodulation distortion elimination of microwave photonics link based on integrated dual-drive dual-parallel Mach-Zehnder modulator. Opt. Lett. 38 (21), 4285–4287.

Jiang, Wei, Tan, Qinggui, Qin, Weize, Liang, Dong, Li, Xiaojun, Ma, Haihong, Zhu, Zhongbo, 2015. A Linearization Analog Photonic Link With High Third-Order Intermodulation Distortion Suppression Based on Dual-Parallel Mach-Zehnder Modulator. IEEE Photonics Journal 7 (3), 1–8.

Stewart II, W.L., Blaylock, J.G., Nov 2004. RF Photonics for aerospace applications. Journal of Aerospace 113 (1), 1629–1640.

Y. Cui, Y. Dai, K. Xu, F. Yin and J. Lin, "Multi-octave operation of analog optical link using parallel intensity modulators," *Optical Communications and Networks (ICOCN), 2013 12th International Conference on*, Chengdu, pp. 1-4, 2013.

Zhu, D., Chen, J., Pan, S., 2016a. Multi-octave linearized analog photonic link based on a polarization-multiplexing dual-parallel Mach-Zehnder modulator. Opt. Express 24 (10), 11009–11016.

A. Agarwal, T. Banwell, P. Toliver and T. K. Woodward, "Predistortion Compensation of Nonlinearities in Channelized RF Photonic Links Using a Dual-Port Optical Modulator," in *IEEE Photonics Technology Letters*, vol. 23, no. 1, pp. 24-26, Jan.1, 2011.

F. V. C. Mendis, M. K. Haldar and J. Wang, "Cross-modulation distortion in subcarrier multiplexed optical systems," in *Proceedings of 1994 Nonlinear Optics: Materials, Fundamentals and Applications*, Waikoloa, HI, USA, pp. 338-340, 1994.

R.G. Walker, N. Cameron, Y. Zhou, and S. Clements, "Electro-Optic modulators for space using Gallium Arsenide," Proc. SPIE 10562, International Conference on Space Optics-ICSO 2016, 105621A, September 2017.

Walker, R.G., Bennion, I., Carter, A.C., 1989. Low voltage, 50Ω GaAs/AlGaAs travelling-wave electro-optic modulator with bandwidth exceeding 25GHz. Electron. Lett. 25 (23), 1549–1550.

W. L. Stewart II and J.G. Blaylock, "The challenge of transmitting super-high-frequency radio signals over short fiber-optic networks on aerospace platforms," 21st IEEE Digital Avionics Systems Conference, Track 4, 4D3, 2002.

Mirza, T.N., Haxha, S., Dayoub, I., 2021. "A Linearized Analog Microwave Photonic Link With an Eliminated Even-Order Distortions," Feb. IEEE Systems Journal. https://doi.org/10.1109/JSYST.2021.3051394.

Zhu, G., Liu, W., Fetterman, H.R., 2009. A Broadband Linearized Coherent Analog Fiber-Optic Link Employing Dual Parallel Mach-Zehnder Modulators. IEEE Photonics Technology Letters 21 (21), 1627–1629.

W. Qin and W. Jiang, "The performance analysis of microwave photonic frequency conversion using double-sideband suppressed-carrier and balance detection," in *IEEE International Conference on Communication Problem-Solving (ICCP)*, pp. 582-585, Guilin, 2015.

C. Middleton and R. DeSalvo, "High performance microwave photonic links using double sideband suppressed carrier modulation and balanced coherent heterodyne detection," MILCOM 2009 – 2009 IEEE Military Communications Conference, Boston, MA, pp. 1-6, 2009.

Kim, J., Johnson, W.B., Kanakaraju, S., Herman, W.N., Lee, C.H., 2009. Demonstration of balanced coherent detection using polymer optical waveguide integrated distributed traveling-wave photodetectors. Opt. Express 17 (22), 20242–20248.

Zhu, Z., Li, Y., Zhao, S., Li, X., Qu, K., Ma, J., 2016b. Broadband linearized analog intersatellite microwave photonic link using a polarization modulator in a Sagnac loop. Appl. Opt. 55 (5), 1022–1028.